Flame-spray interaction and combustion features in split-injection spray flames under diesel engine-like conditions

Wanhui Zhao[1], Lei Zhou[1]*, Ming Jia[2], Zhen Lu[3], Kai Hong Luo[4], Rui Chen[1,5], Haiqiao Wei[1]*

1 State Key Laboratory of Engines, Tianjin University, Tianjin 300072, China

2, School of Energy and Power Engineering, Dalian University of Technology, Dalian 116024, China

3, Clean Combustion Research Center, King Abdullah University of Science and Technology (KAUST), Thuwal 23955-6900, Saudi Arabia

4, Department of Mechanical Engineering, University College London, Torrington Place, London WC1E 7JE, UK

5, Department of Aeronautical and Automotive Engineering, Loughborough University, LE11 3TU, United Kingdom

*Corresponding author: Haiqiao Wei, Lei Zhou

Address: 92 Weijin Road, Nankai District, Tianjin, P. R. China

Tel.: +86-022-27402609

Email: lei.zhou@tju.edu.cn (L. Zhou)

whq@tju.edu.cn (H. Wei)

Abstract

In compression ignition engines, split-injection has shown great benefits in reducing pollutant emissions and improving combustion efficiency. The objective of this study is to investigate flame-spray interaction and combustion features in split-injection spray flames under diesel engine-like conditions. For this purpose, the effects of key injection parameters, including injection duration, dwell times, are investigated. The numerical model is validated by comparing with the experimental data in terms of the vapour penetration length under inert condition and the flame structures under reactive conditions. Good agreement between the predicted and measured data is observed. The effects of the duration of the first injection and the dwell time between the first and second injections on the combustion process are analysed carefully. It is also found that there are different ignition mechanisms for the first and second injections. The chemical explosive mode

analysis (CEMA) method is employed to investigate the autoignition process and flame development for split injections. Different mechanisms are found for the stabilization process.

Keywords: Split -injection; Ignition; Flame-spray interaction; Flame structure;CEMA

1. Introduction

Increasing concern about energy security and environmental pollution has promoted the development of advanced combustion strategies, such as homogeneous charge compression ignition (HCCI), partially premixed compression ignition (PCCI), and reactivity controlled compression ignition (RCCI) [1-3]. These strategies have shown great potential of achieving high efficiency while keeping the harmful emissions low. Multiple-injection technology has been a practically feasible technique in both conventional and advanced combustion by balancing low emissions and high power output [2, 4]. Ignition characteristics and flame lift-off length (LOL) are two of critical factors considered in the design and operation of compression ignition engines. Ignition delay times (ID) determine the combustion phasing, whereas LOL is closely related to the flame stabilization and is of great importance with respect to pollutant emission formation [5].

The main parameters involved in split injection include the pilot injection timing (PIT), pilot injection ratio, dwell time, main injecting timing, and main injection duration. These parameters have great influence on both the torque output and the pollutant emissions. Using either too early a PIT or too late a PIT, the pollutant emissions, including NOx and particulate, and the engine performance can be deteriorated [6]. The proportion of fuel mass injected in the pilot and main injections is crucial in organizing the split-injection strategies. The fuel/air stratification [7] and the subsequent heat release process [8] will be influenced by the injection ratio. Previous study [9] found that the entrainment of oxygen was influenced by the dwell time. By prolonging the interval between the pilot and main injections, entrainment of surrounding oxygen into the flame region was increased and the smoke emissions were reduced. Different conclusion was drawn in [10], in which an endoscopic visualization system was used to investigate the matching between the pilot and main injections with different pilot ratios and dwell times. Only the pilot injection with a small pilot ratio and short dwell time could obtain high thermal efficiency. By increasing the dwell time, the high thermos atmosphere (TA) formed in the pilot injection moved far away from the main injection. As a result, the enhanced evaporation and mixing effects from the TA were restrained. Skeen et al. [11] performed double injections in a constant volume combustion vessel at different ambient temperatures with injection pressure of 150 MPa. Shorter IDs were observed for the second injection because of the entrainment of high temperature gases and intermediate species from the combustion of the first injection. The increase in the pressure and local temperature created favourable conditions for the second injection to ignite earlier [12]. Owing to the fuel-richer ignition and the interaction between the two consecutive fuel injection events, higher soot emission was observed for double injections compared with the single one [13]. Moiz et al. [14-16] performed both experimental and numerical studies to investigate the ignition and quasi-steady combustion process, as well as soot production under diesel engine-like conditions. The results show that by decreasing the initial temperature to 800 K, the production of soot in the first injection was negligible. Hasse et al. [17, 18] applied the representative interactive flamelet (RIF) model for multiple injections. Lim et al. [19] extended the RIF model and only applied the 2-dimensional flamelet equations near the stoichiometric region, finding that the ignition delay for the second injection was closely related to the time for the vapour from the second injection to come into contact with the radicals generated in the first injection. Blomberg et al. [20] compared the combustion process of split injections using a conditional moment closure model (CMC) within the Reynold-Averaged Navier-Stokes (RANS) and Large Eddy Simulation (LES) method, and concluded that the combustion recession at an initial temperature of 900 K could be captured by LES approach, but not for RANS.

Although many experimental and numerical studies have made significant contributions to the combustion process of split injections, the interaction between the first and second injections at different dwell times/injection durations as well as its effect on the combustion characteristics, has not been well analysed. The objective of this study is to investigate flame-spray interaction and combustion features in multiple-injection spray flames under diesel engine-like conditions. For this purpose, the effects of injection parameters, including injection duration and dwell times, on the combustion features of split injection are studied. The novel features of the present work are (1) to investigate the ignition mechanism for the first and second injections; (2) to compare the effect of dwell time, and the first injection duration (FID) on the subsequent combustion process; (3) to explain the development of the flame head for both the first and second injections, and the interaction between the first flame and the coming cold spray; and (4) to study the dominant factor controlling the autoignition and stabilization processes of the second spray. Besides, combustion of the second injection is significantly influenced by the products and intermediate species from the first injection. Analysis on the effect of dwell time (DT) and FID may contribute to the organization of advanced combustion strategies.

The remainder of this article is structured as follows. The numerical approach and experimental setup are briefly presented in Section 2. Section 3 gives the simulated results and discussion, and the conclusions are shown in Section 4.

2. Methodology

2.1 Experimental and numerical setup

Spray experiments have been performed in a constant volume combustion chamber. The test cases are denoted as Spray A in the engine combustion network (ECN) [21]. The fuel injection pressure is 150 MPa, and the fuel temperature is 363 K. The nominal orifice diameter of the injector is 90 μm. The ambient gas density is 22.8 kg/m^3. In the experiments from Skeen et al. [11], a double injection schedule (0.5 ms/0.5 dwell/0.5 ms) was employed at different temperatures. Moiz et al. [8, 16] performed double injections with shorter first and longer second injection durations (0.3ms /0.5 dwell/1.2 ms) to study soot production. Based on their works, double-injection strategies with short and long FIDs were studied at different dwell times. Injection parameters for the investigated cases can be found in Table 1. As advanced combustion strategies always work at low temperature or low oxygen concentration conditions, different injection strategies are adopted at a low initial temperature of 800 K under reacting conditions. The injected fuel mass for the split injections is the same as that in the previous studies [11, 16].

Table 1 Injection parameters.

Case	Duration 1st (ms)	Dwell (ms)	Duration 2nd (ms)
L1	0.5	0.5	0.5
L2	0.5	1.0	0.5
L3	0.5	1.5	0.5
S1	0.3	0.5	1.2
S2	0.3	1.0	1.2
S3	0.3	1.5	1.2

2.2 Flow Solver

The numerical scheme of the employed program is based on the Arbitrary Lagrangian-Eulerian method with finite volume method [22]. For the continuum phase in LES, a third-order Monotone Upstream-centered Schemes for Conservation Laws (MUSCL) [23] is implemented to obtain high order accuracy for the convection term. The MUSCL scheme showed good performance in predicting the non-reacting spray structures and ignition process for reacting jets, as discussed in our previous study [24]. To describe the effects of the filtered small scale turbulence, a k-equation sub-grid turbulent kinetic energy model with $C_{\mu} = 0.067$ and $C_{\varepsilon} = 0.916$ [25] has been implemented, which is named as KIVALES code. The present KIVALES version is further extended to include the linear eddy model (denoted hereafter, as LES-LEM [25]). The LEM model offers a fundamentally different closure for the scalar fields within the contest of LES. In LEM, subgrid turbulent mixing and molecular diffusion processes evolve concurrently in a one-dimensional domain within each LES cell. No parameters are required to adjust to the LES-LEM method [26], and this model has been successfully used in premixed combustion [27], non-premixed combustion [28] and spray combustion [29, 30]. A reduced n-dodecane mechanism including 54 species and 269 reactions [31] is employed. This mechanism shows good ability in predicting the ignition process of n-dodecane spray flames, which has been widely used in previous studies [32-34].

The discrete droplet model (DDM) [22] is applied for the discrete phase. The droplet particles were tracked by solving the droplet velocity, mass, and temperature equations using the Lagrangian method. The Kelvin-Helmholtz Rayleigh-Taylor (KH-RT) model [35] is used to predict the primary and secondary liquid breakup processes. And the O'Rourke [36] model is employed for the simulation of collision and coalescence. The interactions between liquid and gas phases are described through a two-way coupling, i.e. "gas-to-liquid" and "liquid-to-gas". In "gas-to-liquid" coupling, the changes of the droplet velocity in the computation domain are attributed to the drag force $F_{i,d}$ on droplet and calculated by the relative velocity between the droplet and the gas. In the "liquid-to-gas" coupling, the effects of liquid motion on the gas phase are treated as the Lagrangian source terms in the Eulerian momentum equation. Note that in LES the subgrid dispersion velocity model [37] is employed to calculate the effects of turbulent flows on droplets. Furthermore, the spray source term model [38] with a two-test filtering subgrid gas velocity treatment is used to deal with spray effects on the subgrid turbulent kinetic energy. Equations for spray modelling can be found in our previous study [24].

2.3 Comparisons with the experimental data

It should be noted that in our previous study [29], the simulated distributions of the mixture fraction at different times and locations by the present numerical methods were compared with the experimental results, and good agreements between the predicted and measured results were obtained. We have compared the vapor penetration length for inert n-dodecane spray with the experimental data in our previous study [30]. The present numerical model coupled with the high-order MUSCL scheme can give a reasonable agreement with the experimental data. We have also examined the quality of the performed LES by comparing the results from different realizations [39]. Results calculated by the ratio of resolved and total turbulent kinetic energy (TKE) illustrated that high-levels of TKE could be resolved, especially at downstream positions. Although the turbulent fluctuations are not completely resolved, the numerical model does not change the main conclusion.

To further validate the numerical model under reacting conditions, comparisons of experimental images from planar-laser-induced fluorescence (PLIF) and the Schlieren images with the simulated results for the reacting sprays are shown in Fig. 1 at an initial temperature of 800 K to further show the performance of the present models. The experimental ID for the first injection is 0.88 ± 0.09 ms from pressure profile. In this work, ID is defined as the time when the maximum temperature in the entire domain reaches the ignition temperature T_{ign}, which is calculated by $\mathrm{T}_{ign} = 0.5 * (T_{amb} + T_{max})$ [40]. T_{amb} is the initial ambient gas temperature, and T_{max} is the maximum temperature during the quasi-steady state. The predicted ID is 0.895 ms for the first injection. The experimental images show the distribution of polycyclic aromatic hydrocarbons (PAH) and formaldehyde (CH_2O) molecules. However, for the simulation, PAH is not included in the chemical kinetic mechanism, and acetylene (C_2H_2) is employed to represent the formation of soot. Therefore, CH_2O and C_2H_2 are used to give a qualitative comparison with the experiments. At 890 μs, the second injection has not commenced yet. Strong PLIF signal appears in the firstly injected spray, and very weak colour appears in the Schlieren image. Skeen et al. [41] pointed out that during the low-temperature ignition stage, when the local temperature is close to the ambient gas temperature, the gradient in the local refractive index is reduced, and a “softening” effect near the head of the spray is observed. Consistent with this conclusion, high levels of CH_2O appear at the reacting spray head in the predicted result, and the decrease in the gas density is very slight at 0.9 ms. At 1290 μs, high-temperature reactions occur in the spray, leading to significant reduction in gas density, as shown in the Schlieren image. The simulated result overestimates the reacting spray head for the first injection, while the position of the second spray or the second spray head agrees well with the experiments.

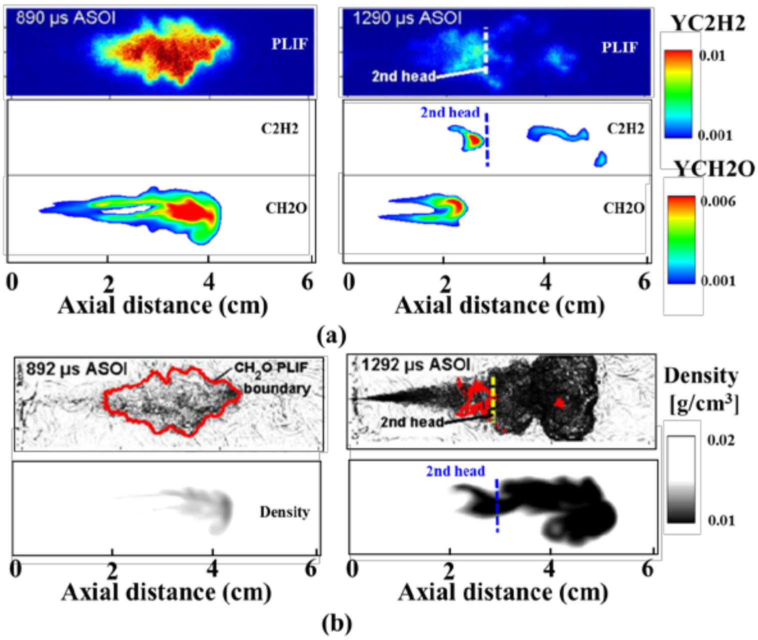

Fig. 1. Comparisons of (a) modelled results with (b) PLIF and Schlieren experimental images at an initial temperature of 800 K. Experimental data are from Skeen et al. [11].

3. Results and discussion

3.1 Effects of dwell time on combustion processes.

3.1.1 Analysis of ignition process

Previous study [16] showed that the dwell time has a great influence on soot formation. In this section, the autoignition process for the double injections with a FID of 0.5 ms is further analysed, and meanwhile, the combustion process at different dwell times (DT) is mainly investigated. The temporal evolutions of key species in the temperature versus mixture fraction (Z) space are shown in Fig. 2, including CH_2O and hydroxyl (OH). Z is calculated based on the mass fraction of C and H atoms [42]:

$$\mathrm{Z} = \sum_{\alpha=1}^{Ns}(MW_C\, n_{C,\alpha} + MW_H\, n_{H,\alpha}) \times Y_\alpha/MW_\alpha \tag{1}$$

where MW_C, MW_H, and MW_α are the molecular weights of carbon atoms, hydrogen atoms, and species α, respectively. Ns is the total number of species. $n_{C,\alpha}$ and $n_{H,\alpha}$ are the number of carbon and hydrogen atoms, respectively. Y_α is the mass fraction of species α. It is noted that only points with $Y_i > 20\% \times Y_i^{max}$ are shown in Fig. 2, where Y_i is the mass fraction of species i, and

Y_i^{max} is the maximum value of Y_i. As mentioned above, autoignition appears after the end of the first injection and before the start of the second injection. Therefore, before the start of the second injection, the autoignition process of the first injection for the cases with long DTs (Cases L2 and L3) is nearly the same as that with short DT. CH_2O can be used as an ignition precursor [43]. After the end of the first injection, amount of air is mixing with the spray from all around of the spray. The entrainment of fuel is improved. As a result, no very rich mixture is left in the spray, and mixture fraction is less than 0.1 in the computational domain, but autoignition is still initiated at the place with mixture fraction greater than stoichiometry. In addition, Fig. 2 also shows that OH and CH_2O are located at different places in the T-Z space. OH is mainly formed at high temperature regions with stoichiometric mixture fraction (Zst), and CH_2O is distributed over a wider region in the mixture fraction space at low temperature regions.

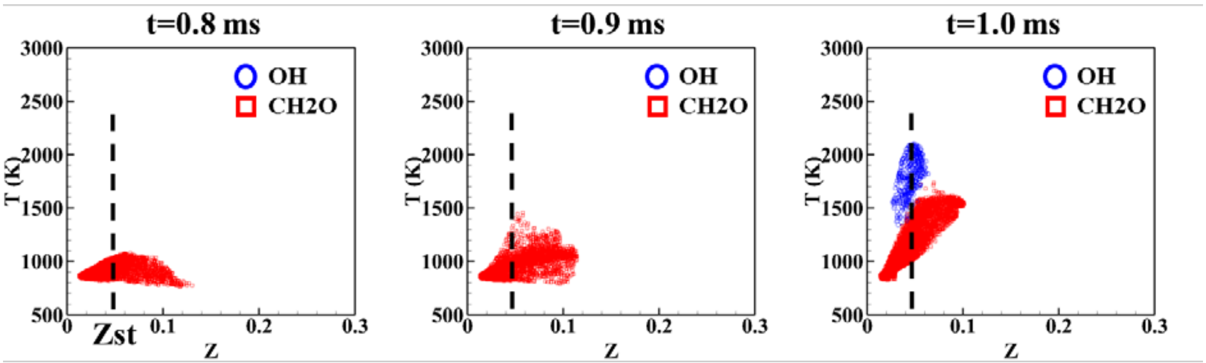

Fig. 2. Ignition process for the first injection with injection duration of 0.5 ms. The black dashed line represents the stoichiometric mixture fraction (Zst).

It should be noted that the second injection starts at later times after the start of injection (ASOI) with a long DT. The effect of dwell time on the ignition of the second injection at different times after start of the second injection (ASSI) is shown in Fig. 3. Key intermediate species, including OH and CH_2O, are plotted in T-Z space at times relative to the start of the second injection. By increasing the DT, the second shot is injected into combustion chamber under different conditions involving temperature, and charges chemical composition compared with the case with a short DT. For a short DT, for example at DT=0.5 ms, the second injection penetrates into intermediate products and experiences first-stage ignition with an advanced timing, as reported in the experimental study [11]. At 0.1 ms ASSI, CH_2O appears in the near-injector region, which is characterized by low temperature and different values of Z. At 0.2 ms ASSI, temperatures in the cells of fuel-rich regions increase to 1500 K approximately, indicating that ignition process for the second injection is initiated very quickly. By increasing the dwell time, combustion process has been sustained for a longer time, and consumption of fuel from the first injection is more complete at the time when the second injection starts. As a result, the effect of intermediate species on ignition of second injection becomes minor. By increasing the DT, most of CO is converted to CO_2 during the high-temperature ignition stage by $CO+OH \rightarrow CO_2+H$ [44]. Thus, more CO_2 is formed in the entire domain, and due to diffusion, CO_2 is located in a wider region. Interestingly, the increase in the CO_2 production and temperature generated by the first injection plays an important role. CO_2 production can delay the high-temperature ignition of the second injection, and on the contrary, the increased temperature promotes the ignition process. Once the cold second injection penetrates into the already burnt region, the fuel spray is surrounded by CO_2 to prevent the high-temperature ignition. Moreover, due to the increased time before the first and second injections starting to interact with each other at a longer DT, ignition is prolonged for the second injection.

For example, in the case with DT=1.5 ms, both OH and CH_2O mass fractions are lower than 20% of the maximum value at 0.1 ms ASSI. The appearance of high-temperature products like OH is delayed by increasing the dwell time. The tail of the first injection has moved further downstream, and thus more time is needed for the second injection to catch up with the tail of the first injection. After the two injections start to interact with each other, high-temperature reactions occur in the second spray quickly. Therefore, the fuel/air mixing for the second injection strongly depends on the interaction time before high-temperature ignition. Moreover, more oxygen is entrained into the burnt region by increasing the DT. Consequently, the prolonged interaction time and the entrainment of oxygen into the burnt region in the first injection lead to the improved mixing process with a long DT. As a result, the high-temperature kernels appear in fuel-leaner regions compared with a short DT (case L1). Moreover, distributions of OH in T-Z space become very sparse at long DT, indicating that the high-temperature reactions are weaker than that at the same time interval in the cases with short DT. Hence, it can be concluded that the interaction between the first and second injections is reduced with a longer DT. If the interval between the two injections is long enough, the interaction between the two pulses can be avoided [45]. Due to the less fuel-rich regions and the improved mixing between fuel and air, soot emission can be reduced by increasing the DT [16].

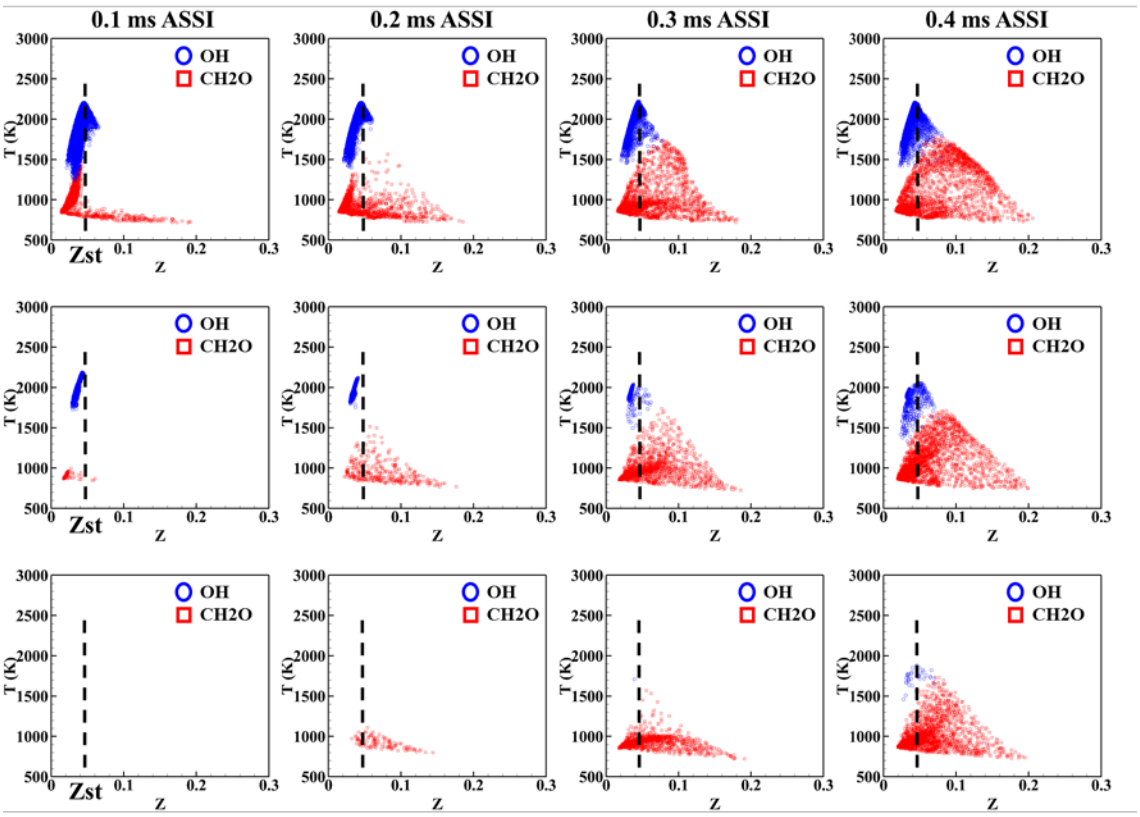

Fig. 3. Combustion process at different times after start of the second injection (ASSI). Top: DT=0.5 ms, Middle: DT=1.0 ms, Bottom: DT=1.5 ms. The black dashed line represents the place of Zst.

Temporal evolution of the scatters of reaction region (RR) in the mixture fraction space is shown in Fig. 4 at different times ASSI. RR is calculated by $RR = Y_{CH2O} \times Y_{OH}$. As reported in the previous studies, RR can show the flame structures [46, 47] and mark the ignition process [29]. It can be seen in Fig. 4 that RR in fuel-rich regions increases gradually with time for all dwell times, indicating that strong chemical reactions move from stoichiometric regions to fuel-rich regions, where high levels of CH_2O appear. As the flame LOL is reduced for the second injection, the intense reactions occur quickly after the fuel injection. CH_2O is formed in fuel-rich regions due to the limited mixing process, leading to high values of RR thereby. As reported in the previous study [43], intense high-temperature reactions occur at the stoichiometric mixture fraction, where high levels of OH are formed. OH formation is dominant. Consequently, the maximum value of RR moves to stoichiometric mixture fraction during the quasi-steady state of a single injection [29]. The results for double injections show similar characters with the maximum RR at Zst. The ignition process is advanced for the second injection, and fuel-rich ignition is observed. Furthermore, it can also be seen that by increasing the dwell time, value of RR at early times is reduced. This is because that the reaction region in the first injection have moved downstream at a high velocity, and only a small quantity of OH and CH_2O left behind the tail of the first spray, as shown in Fig. 3.

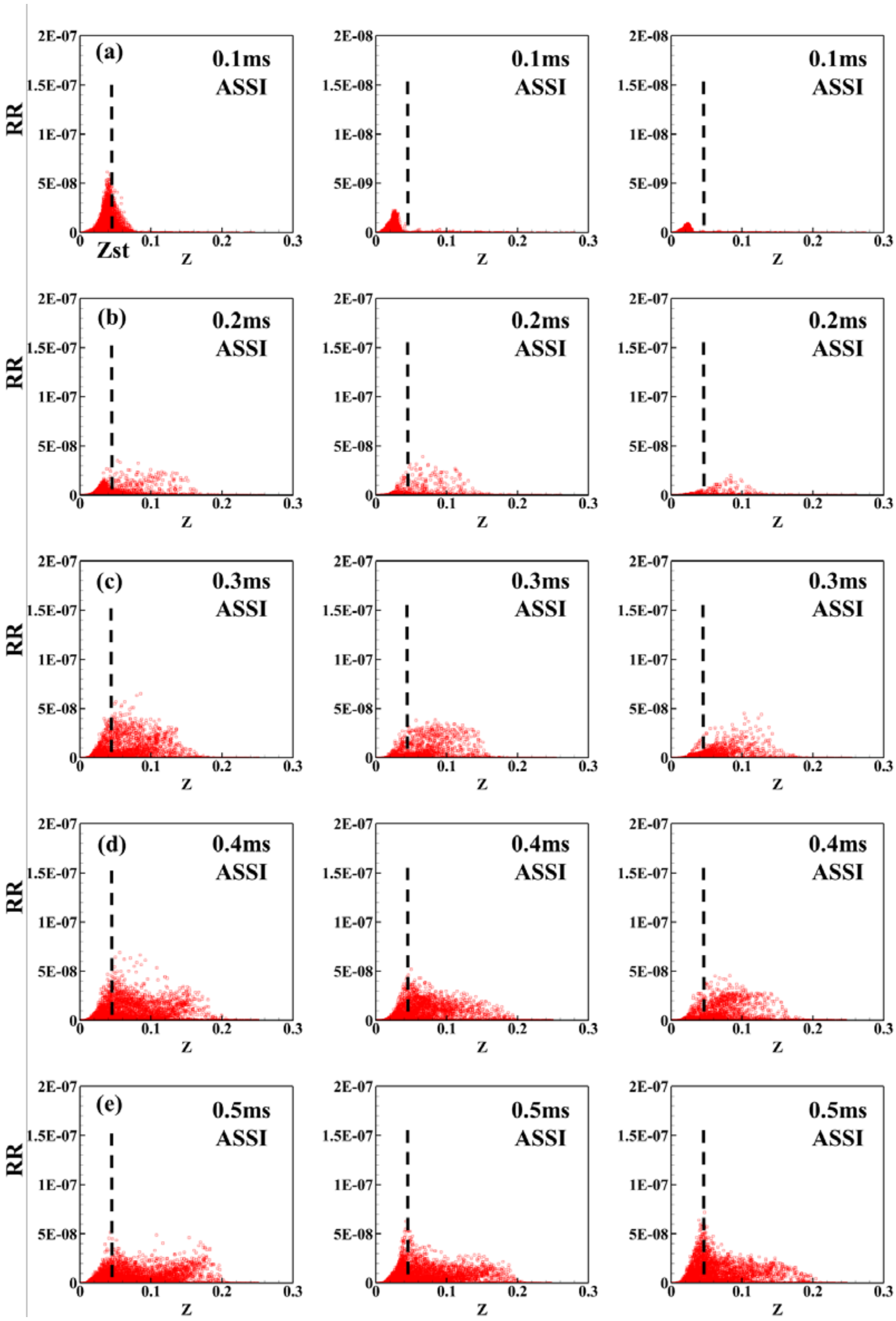

Fig. 4. Temporal evolution of reaction region (RR) with different dwell times. (Left) DT=0.5 ms, (Middle) DT=1.0 ms, (Right) DT =1.5 ms. RR is calculated by $RR = Y_{CH2O} \times Y_{OH}$. The black dashed line represents Zst.

3.1.2 Analysis of penetration length and flame LOL

To further discuss the effect of injection dwell time on spray-flame interactions and the development of the spray tip, Fig. 5 shows the evolutions of the spray tip for the first and second injections. To distinguish the two injections, the reacting spray tip of the first injection is defined as the most downstream place with mixture up to 0.01. The second spray tip is defined as the farthest distance between the location of Z reaching stoichiometry and the injector. Similar definitions can be found in [12]. It is clearly shown that the flame tip position for the first injection is quite similar with different dwell times before 1.7 ms. At DT=0.5 ms, the spray tip for the first injection is accelerated after 1.7 ms due to the coming of the second injection, which could provide high momentum for the first injection [14]. However, for longer DTs, the tip of the second injection has not merged with the first one, and the momentum for the first tip is very weak. For the second injection, it is injected into a low density environment due to the combustion. Decrease in the gas density leads to gas expansion [11]. The second spray tip moves faster than the first one. Note that at t=1.2 ms, for the case with DT=0.5 ms, the tip of the second spray catches up with the tail of the first injection (not shown here). Fuel is injected into a hot environment with rich radicals. The transport of intermediate species and radicals leads to the acceleration of the second spray tip. For longer dwell times, when the second tip catches up with the first injection, the fuel is almost completely consumed. The acceleration of the second tip due to the first injection is not as obvious as that in the case with short dwell time.

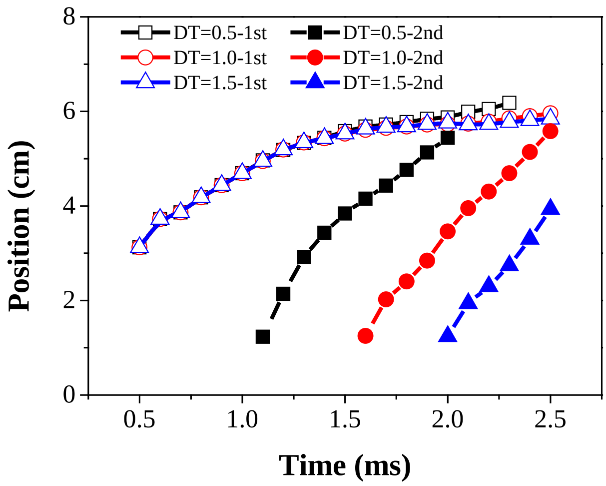

Fig. 5. Temporal evolutions of spray tip.

Temporal evolutions of flame LOL with different dwell times are shown in Fig. 6. To compare the effect of dwell times on flame LOL, the result from a single injection with 1.5 ms duration at an initial temperature of 800 K is also shown in Fig. 6. The simulated flame LOL for single injection is close to 30 mm, which is slightly longer than the experimental result (26.2 mm) [21]. For double injections, obvious decrease in flame LOL can be observed because the tail of the first injection comes into the reaction during the dwell time owing to the mixing between fuel and fresh air. The combustion recession was seen at a higher temperature in the experiments [11]. After the start of the second injection, shown as points A', B' and C' in Fig. 6 for different dwell times, flame LOL is prolonged very quickly, indicating that the second tip catches the tail of the first injection. Owing to the cooling effects from the cold spray, the flame LOL moves downstream. After the appearance of high-temperature reactions in the second injection, flame LOL is shortened and high-temperature regions move upstream again.

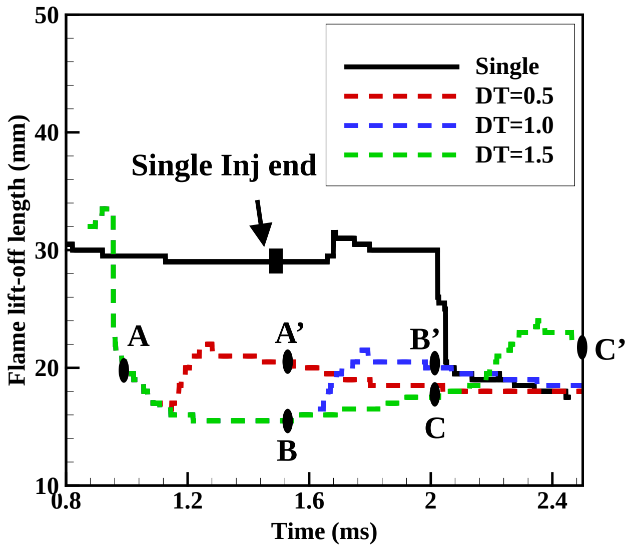

Fig. 6. Flame LOL at an initial temperature of 800 K. A, B and C: Start of the second injection. A', B' and C': End of the second injection.

3.1.3 Analysis of ignition mechanism

To compare the flame development for the first and second injections, temporal evolutions of CH_2O mass fraction, axial velocity, and temperature profiles at the second spray tip are shown in Fig. 7. Lines without and with symbols represent the time interval ASOI and ASSI, respectively. At 0.3 ms, autoignition for the first ignition has not occurred. The injected fuel is evaporating, and thus temperature at the spray tip is very low. Recently, Desantes et al. [48] investigated the transient spray tip under non-reacting and reacting conditions, finding that during the early time without the formation of high-temperature kernels, position of the spray tip is quite similar. In this work, ignition delay is shortened for the second injection. Comparisons of the spray tip for the first and second injections could show the effect of combustion. Moreover, because of the earlier ignition in the second injection and the reduction in the gas density ahead of the second injection resulting from the combustion of the first spray, it could show the acceleration in the second injection, as discussed above. Furthermore, the second spray is injected into a higher-temperature environment with different intermediate species, and different mechanisms may dominate the ignition process for the first and second injection. As shown in Fig. 7, the temperature of the second spray tip is much higher than the first injection. Owing to the limited mixing time and high temperature in the gas, richer ignition is formed. Thus, high levels of CH_2O exist ahead of the second injection. The consumption of CH_2O also indicates the appearance of high-temperature reactions [43]. At later times, high-temperature reactions appear ahead of the second spray and CH_2O is consumed by OH and other radicals, consistent with the temperature increase thereby.

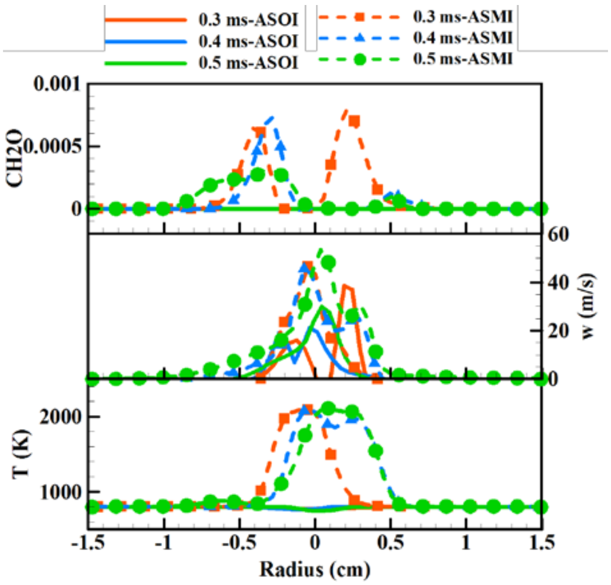

Fig. 7. Comparisons of CH_2O mass fraction, axial velocity, and temperature for the first and second injection spray heads.

To further study the effects of dwell time on the ignition process of the second injection, temporal evolutions of temperature and key species mass fraction at different times ASSI are shown in Fig. 8. In the case with short dwell time, for example DT=0.5 ms, temperature increase at the second spray tip at 0.1 ms ASSI is small and the highest temperature at the inner side is below 1000 K. However, at 0.2 ms ASSI, the maximum temperature at the inner head is more than 2000 K, indicating the appearance of high-temperature reactions. High concentration of CO and OH is observed, and the mass fraction of the ignition precursors, such as CH_2O, H_2O_2, and hydroperoxy (HO_2), decreases quickly. By increasing the dwell times, more time is needed for the second injection to catch up with the first one, and low levels of species are left behind the first injection, as discussed in Fig. 3. The temperature at the inner spray tip is lower, and species concentration at the inner spray tip is smaller at 0.1 ms ASSI. The time when the maximum temperature at the inner spray head increases above 1800 K is delayed. Then in the case with DT=1.5 ms, high value of OH is observed even later than 0.3 ms ASSI, indicating that the ignition delay of the second spray is prolonged for longer dwell time.

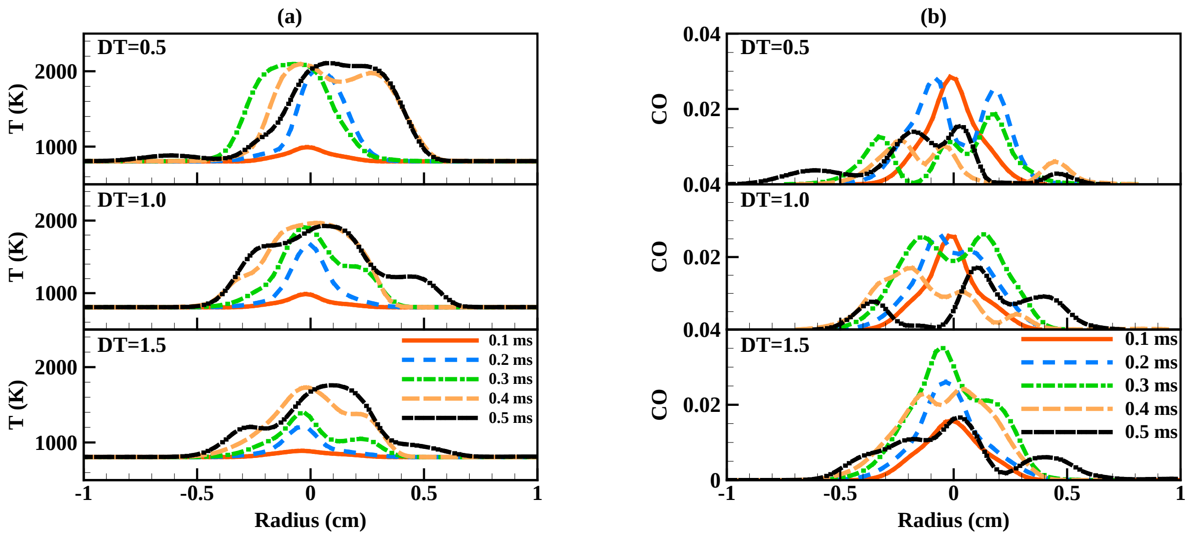

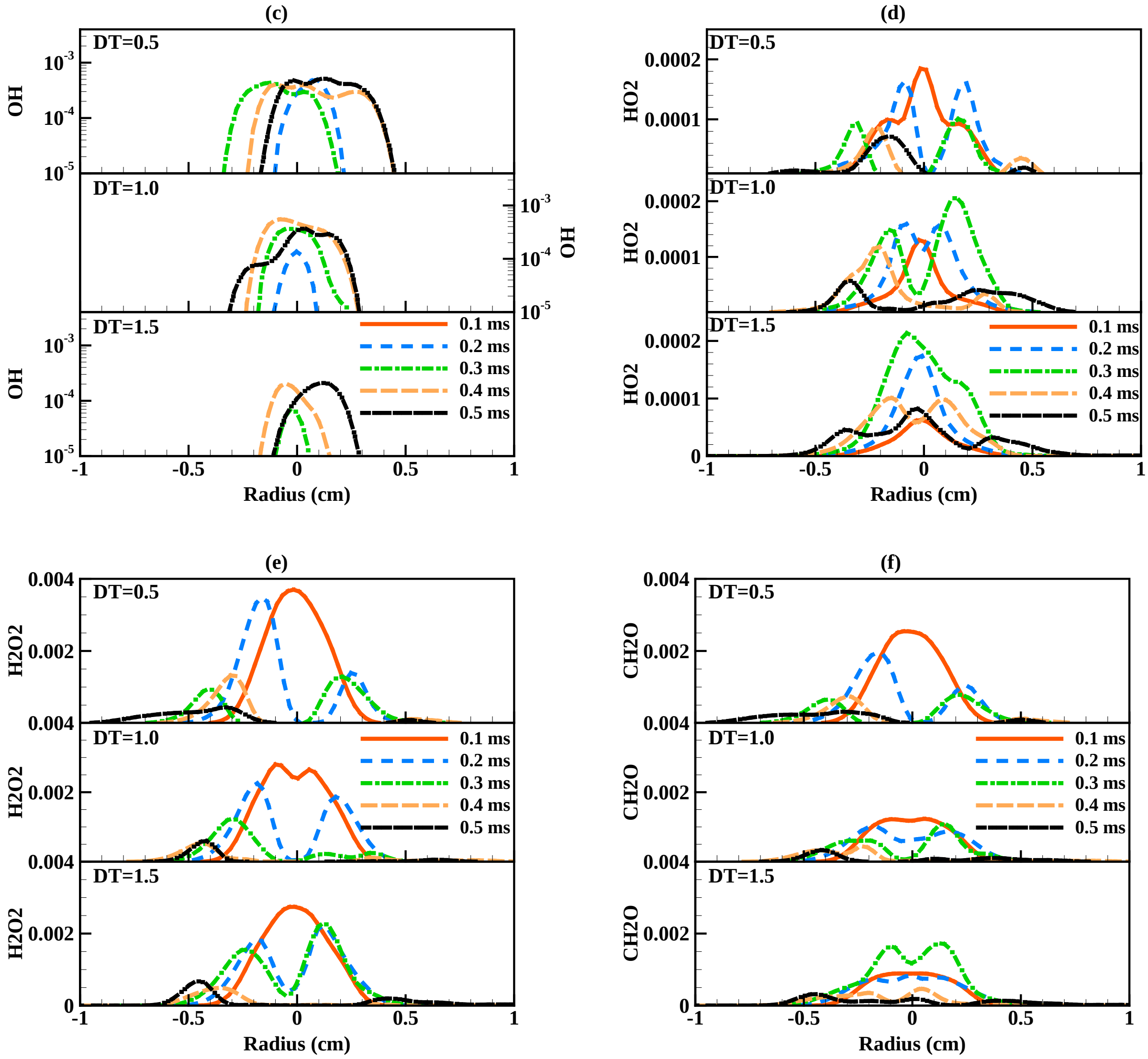

Fig. 8. Temporal evolutions of temperature (a), equivalence ratio (b) and key species at the second spray head after start of second injection with long injection durations.

To further investigate the ignition mechanism for the second injection, different cases for homogeneous reactor with $C_{12}H_{25}O_2$, CH_2O, H_2O_2, or OH additions are shown in Table 2. As a large amount of oxygen is consumed by the first injection, the effects of species addition on the ignition process at low oxygen concentration are investigated. The initial temperature for homogeneous reactor is chosen based on Fig. 8, in which the temperature at the second spray tip is slightly increased at 0.1 ms ASSI. Meanwhile, as reported in [11], pressure rise is very little. Therefore, the initial pressure for the cases shown in Table 2 is set to 5.25 MPa, equal to the initial pressure for the 3-D constant volume combustion vessel. The predicted ignition delay times in the temperature versus equivalence ratio space without species addition are shown in Fig. 9 using CHEMKIN[49]. The predicted IDs with values of 0.1 ms and 1.0 ms imply the mixture with short and long IDs, as shown in Fig. 9. It shows that n-dodecane exhibits a negative temperature coefficient (NTC) regime in the region with temperature ranging from 900 to 1100 K and equivalence ratio smaller than 2. At the regions with temperature lower than 800 K, ID is longer than 2.0 ms at different equivalence ratios.

Table 2 Ignition process for homogeneous reactor.

T (K)	P (MPa)	O_2 (%)	Addition / (%)
700~1300	5.25	10	No addition
		10	$C_{12}H_{25}O_2$: 0.01; 0.05
		10	CH_2O / 0.1; 0.5
		10	H_2O_2 / 0.1; 0.5
		10	OH/ 0.01; 0.05

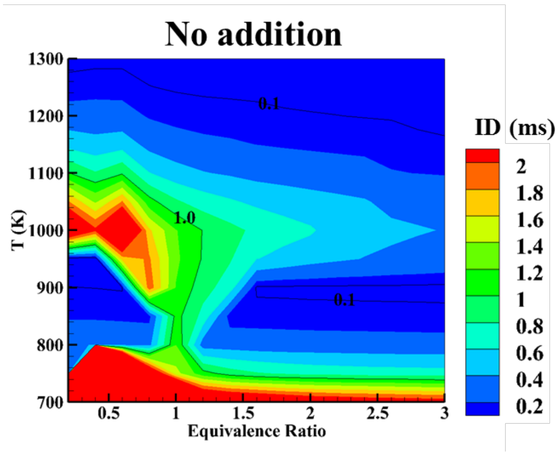

Fig. 9. Predicted IDs at different temperatures and equivalence ratios without species addition.

When the second injection starts, it is penetrated into a hot environment with different species formed in the first injection, such as $C_{12}H_{25}O_2$, CH_2O, H_2O_2, OH and so on. To study the effect of these species on the ignition process, comparisons of the IDs with different species addition are shown in Fig. 10. $C_{12}H_{25}O_2$ is one of the key species in the low-temperature reactions through the O_2 addition to the R radical. CH_2O can be used to mark the cool flame, H_2O_2 is decomposed intensively once temperature increases over 1000 K [44]. Comparing Fig. 9 and Fig. 10, it can be seen that ID is reduced in the low temperature regions by adding small amount of $C_{12}H_{25}O_2$. At the regions with temperature greater than 800 K, the effect of $C_{12}H_{25}O_2$ addition on ID is insignificant, especially for the fuel-rich mixtures. $C_{12}H_{25}O_2$ is mainly formed in the low-temperature reactions. The appearance of $C_{12}H_{25}O_2$ promotes the low-temperature chemistry, and the production and decomposition of ketohydroperoxide ($OC_{12}H_{23}OOH$) are also promoted [44]. The overall rate of the low-temperature combustion is enhanced. Once CH_2O is added, autoignition timing for the mixture with temperature lower than 950 K is prolonged. Owing to CH_2O addition, the times when the ketohydroperoxide starts to form, and when the temperature starts to increase quickly are delayed. The maximum $OC_{12}H_{23}OOH$ mole fraction is also reduced, indicating that the low-temperature reaction path is restrained with the addition of CH_2O. For the fuel-rich mixture with temperature above 1200 K, the effect of CH_2O addition on the ID is negligible. Similar to CH_2O addition, the existence of H_2O_2 in the initial gas prolongs the ID at low initial temperatures. For the mixture with temperature above 1000 K, the decomposition of H_2O_2 is promoted through the chain-branching reaction $H_2O_2+M \rightarrow OH+OH+M$. The temperature rise appears earlier and a reduction in ID is observed. As shown in Figs. 10 (g) and (h), IDs are significantly reduced through the addition of OH, especially for the mixture with equivalence ratio greater than 1.5, and most of the mixture has a ID lower than 0.1 ms with 0.05% addition of OH. However, OH is mainly formed in high-temperature regions. The production of amount of OH in the second spray still needs more time due to the limited mixing between fuel and air. After about 0.2-0.3 ms ASSI, high-temperature reactions appear in the first spray, where high concentration of OH is formed. Once the second spray catches up with the first one, significant reduction in ID can be observed. Hence, it can be concluded based on Fig. 10 that the existence of CH_2O and H_2O_2 prolongs the ID at low temperatures. Although the existence of $C_{12}H_{25}O_2$ shortens the ID, this effect is very limited. The addition of OH significantly reduces the ID, especially for the rich mixture. In spray flames, amount of OH has formed quickly after the start of the second injection. Once the first and second injections get to interact with each other, the existence of OH in the first spray can ignite the second injection. Therefore, the second injection is ignited by the first one.

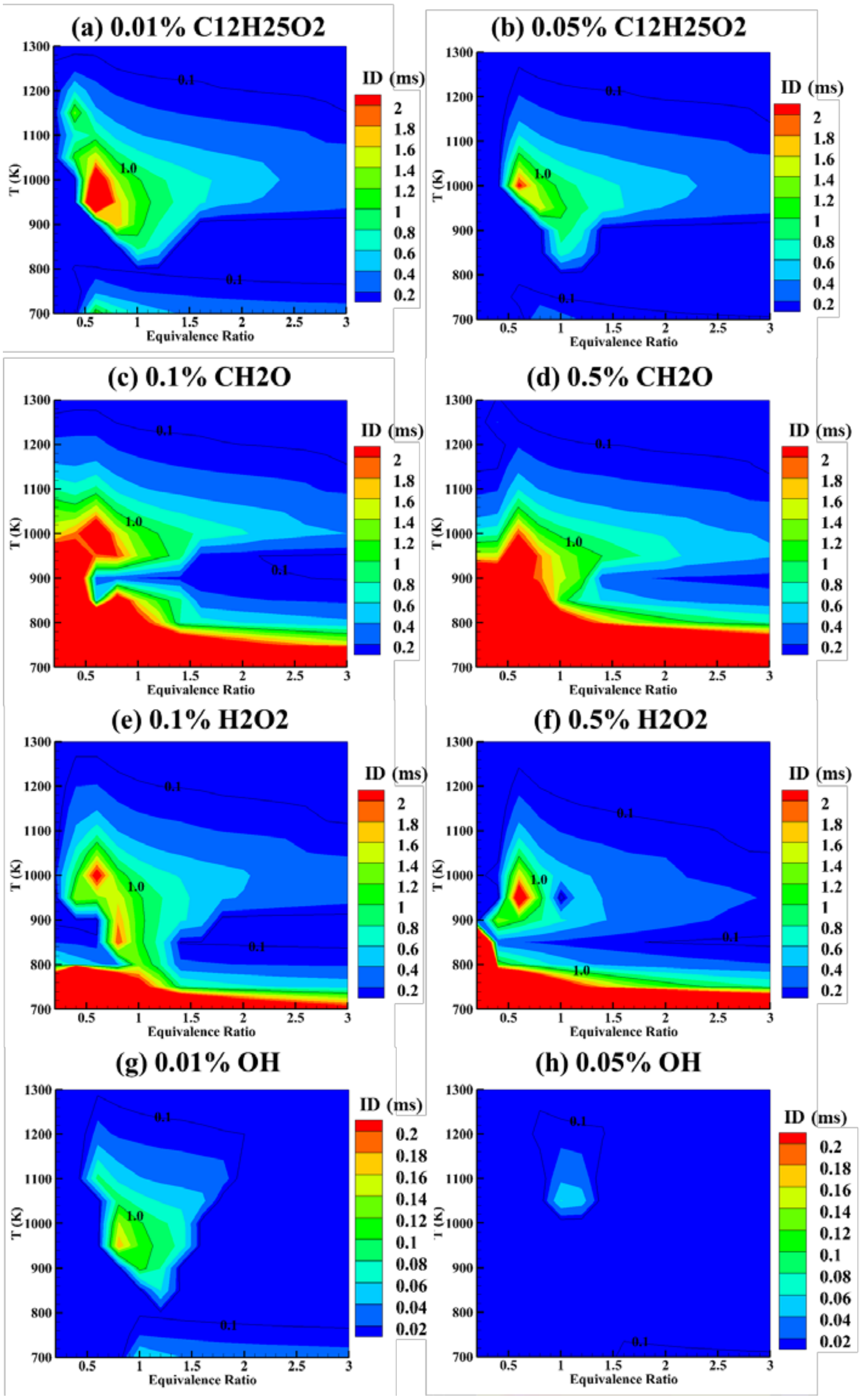

Fig. 10. Predicted IDs with different species addition.

3.2 Combustion process with long and short durations.

The injected fuel mass or injection duration for the first injection is of great importance to improve fuel stratification [7], optimize the combustion phasing [8], and reduce soot emission [50, 51]. Therefore, in order to optimize the combustion process, the ignition process for double injections with different FIDs should be further analysed in detail. Fig. 11 shows the scatters in the temperature versus mixture fraction space with different dwell times at a short FID. As shown in the figure, by decreasing the FID, the injected fuel mass is reduced at an injection pressure of 150 MPa. Similar conclusion can be found by increasing the DT with long and short FIDs. OH and CH_2O mass fractions are weaker at longer DTs. The fuel/air mixture in the first injection becomes leaner than that at a long FID at the autoignition timing due to the lack of fuel. Before the start of the second injection, mixture becomes very lean. Thus, OH is mainly formed in fuel-lean regions. After the second injection starts, fuel-rich mixture is formed to support the production of CH_2O. Although CH_2O is found in fuel-lean regions, most of them are still formed in fuel-rich regions in the inner side of the second injection. It should be also noted that compared to the cases with long FIDs, the second injection starts much earlier than the case with the same DT and a long FID, as shown in Fig. 3. The first injection has burned for a shorter time. Therefore, there are many cells with OH mass fraction greater than the 20% of the maximum value at 0.1 ms ASSI with DT=1.5 ms. Then at 0.3 ms ASSI, combustion of the first injection is more complete. Thus, OH mass fraction is very weak. The appearance of OH mass fraction around Zst is again attributed to combustion of the second injection.

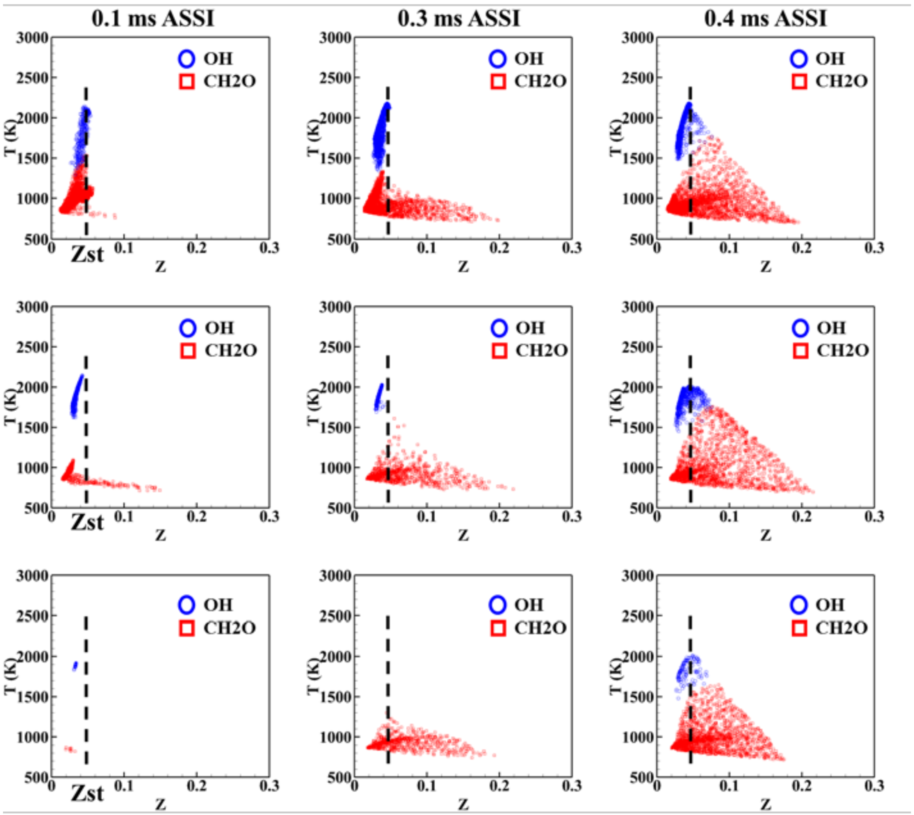

Fig. 11. Ignition process for the second injection with a short FID. Top: DT=0.5 ms, Middle: DT=1.0 ms, Bottom: DT=1.5 ms. The black dashed line represents the location of Zst.

To further compare the combustion process with long and short FIDs, temporal evolutions of the mean temperature and apparent heat release rate (AHRR) are shown in Fig. 12. It can be seen that due to the combustion of first and second injections, the mean temperature in the entire computational domain is increased. With earlier start of the second injection, the time when the profiles of T_{mean} continue to increase occurs much earlier. What's more, there are mainly two peaks in the AHRR profiles. The first peak is due to the premixed combustion of the first injection, while the second one is related to the consumption of the fuel injected during the second injection. For the cases with long FIDs, more fuel is injected into the computational domain. The first peak for the maximum AHRR before 1.2 ms is higher than the case with a short FID due to the premixed combustion of the first injection. For the cases with a short FID, fuel/air mixture becomes very lean before the wide consumption of fuel, and a low AHRR peak is observed due to the lack of fuel. And most of heat is released after the start of second injection during which more fuel is injected into the combustion chamber. By increasing the DT, the peak AHRR appears much later. The time when the second injection starts has great influence on the formation of CH_2O and the evaporated fuel mass, as shown in Fig. 13. Amount of CH_2O is formed in the first spray both for the cases with long and short FIDs. Once the high-temperature kernels appear, consumption of CH_2O leads to the decrease of CH_2O mass [43]. It can also be seen in Fig. 13 that at the time when fuel mass starts to decrease, CH_2O mass in the entire combustion chamber starts to increase, indicating that n-dodecane is mainly consumed by the cool flame in the first injection. Once the second injection begins, the increase of the accumulated CH_2O mass profiles is not as quick as that in the first injection, indicating that the cool flame is not as obvious as that in the first flame. As the ignition delay for the second injection is reduced compared with in the first injection, the injected fuel goes into the high-temperature regions quickly. The high-temperature environment promotes the evaporation of fuel droplets and the appearance of high-temperature reactions in the second injection. The consumption of fuel in the high-temperature reactions plays a dominated role.

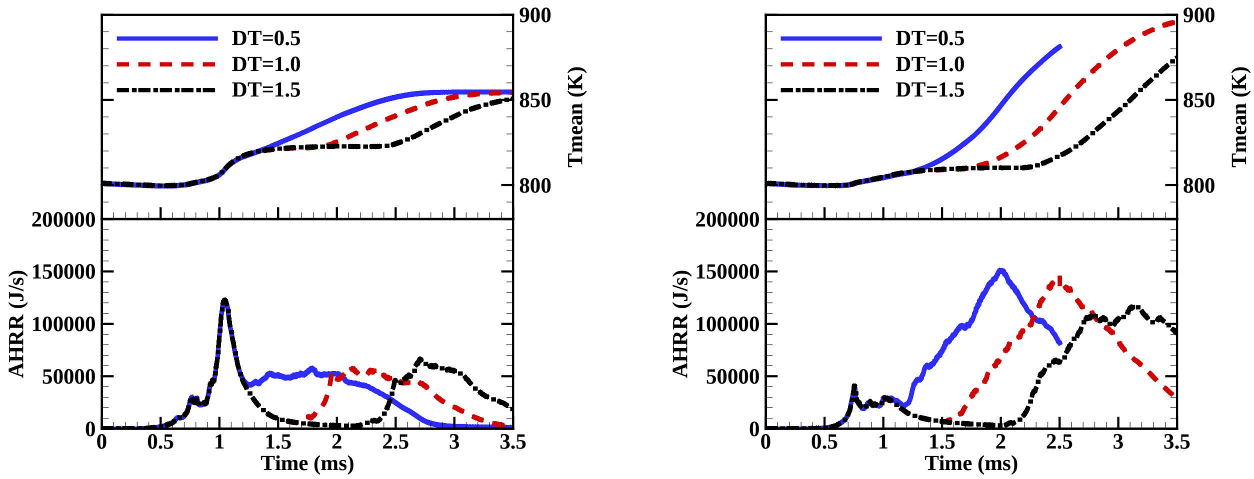

(a) FID=0.5 ms (b) FID= 0.3 ms

Fig. 12. Temporal evolutions of mean temperature (T_{mean}) and apparent heat release rate (AHRR).

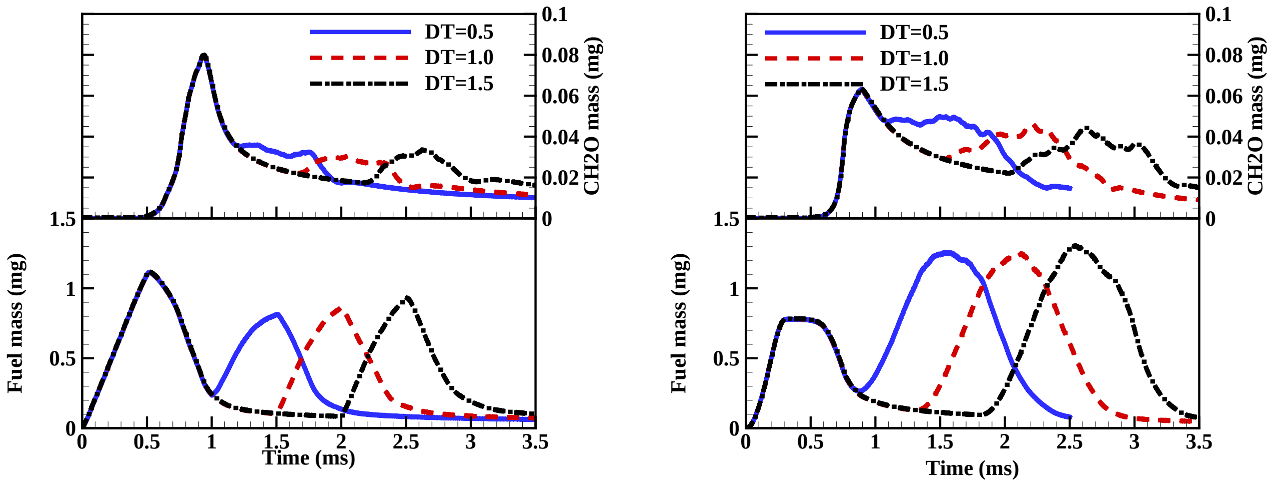

(a) FID= 0.5 ms (b) FID= 0.3 ms

Fig. 13. Temporal evolutions of fuel and CH_2O mass.

To further show the effect of DT on the combustion process of n-dodecane spray flames, the distributions of temperature, mass fraction of fuel and oxygen along axial direction are shown in Fig. 14. It should be noted that profiles are extracted along the centre line of z axis. The high-temperature regions mainly represent the combustion region in the first spray. It can be seen that for the case with a long DT, the flame length is longer, characterized by a longer high-temperature region. Oxygen concentration in the high-temperature regions is also larger than that in the other two cases with short DTs. This is because that although the oxidizer is consumed by the combustion of the first injection, the reduction in density due to gas expansion leads to the entrainment of O_2 from the ambient gas to support the oxidization of the fuel for the second injection. By comparing the cases with the same DT and different FIDs, temperature at the flame front is reduced with short FIDs because of the over-mixing between fuel and air in the first injection, as shown in Fig. 14. Mixture becomes too lean, and the combustion temperature drops obviously. Comparisons of the flame structures at different dwell times are shown in Fig. 15. It can be seen that the flame tip has moved downstream freely with less time for the cases with short FIDs, and thus, the second spray head could catch up with the first flame much earlier compared to the cases with longer FIDs. The first and second flame heads have merged before 2.0 ms ASOI, but there is a small gap between the first and second flame heads for the case with DT=0.5 ms, as shown in Fig. 15 (a). By increasing the DT, the maximum temperature in the first flame is reduced at the same time ASOI, and ignition of the second injection is delayed in the cases with longer DTs.

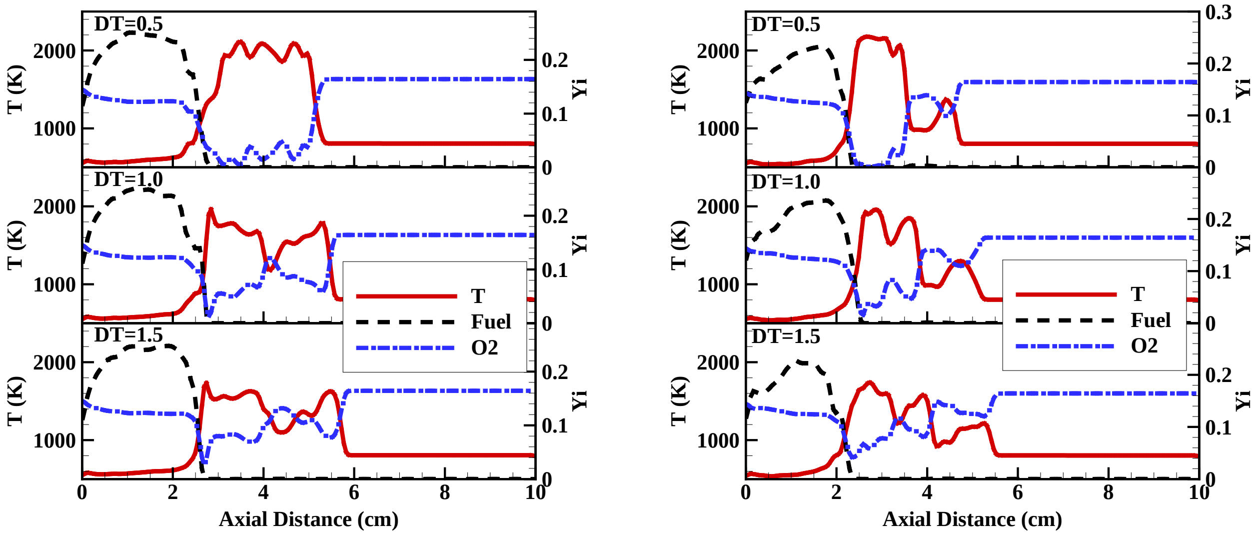

(a) FID= 0.5 ms (b) FID= 0.3 ms

Fig. 14. Profiles of instantaneous T and Z along the centre axis at 0.4 ms ASSI with long and short FIDs.

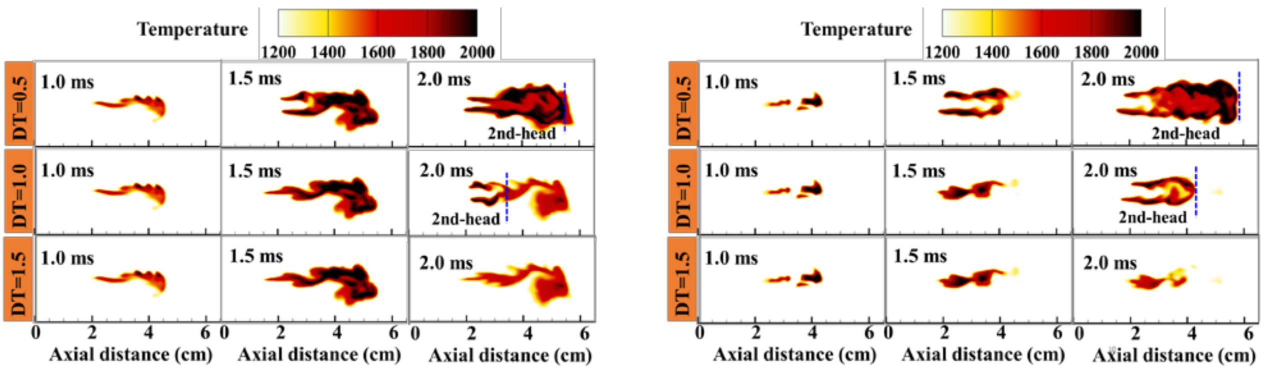

(a) FID= 0.5 ms (b) FID= 0.3 ms

Fig. 15. Temperature contours at different times ASOI with (a) long and (b) short FIDs.

3.2 The stabilization mechanism for double injections

Chemical explosive mode analysis (CEMA) is employed for the study of the development of n-dodecane spray flame using different injection strategies. CEMA was shown to be a robust diagnostic of complex fields and it can be used to predict the important flame features, such as ignition, extinction, and flame fronts [52-55]. In this study, CEMA method is briefly summarized.

The Jacobian of the chemical source term, $\mathbf{J}_\omega$, in the governing equations can be used to account for the local chemical characteristics. $\mathbf{J}_\omega$ is calculated by $\mathbf{J}_\omega = \partial\boldsymbol{\omega}/\partial\boldsymbol{y}$, where $\boldsymbol{\omega}$ represents the chemical source term, and $\boldsymbol{y}$ is the vector of species concentration and temperature. A chemical explosive mode (CEM) is known as the state with $Re(\lambda_e) > 0$. A large positive eigenvalue indicates an explosive mixture, and autoignition is underway. While negative values for Λ_e mean the mixture already ignited. The transition of a CEM from explosive, i.e., $Re(\lambda_e) > 0$, to non-explosive, i.e., $Re(\lambda_e) < 0$, can be regarded as a flame front or flame surface [53, 56]. CEMA focuses on the unique features of the CEM, which is derived from the all of the species concentration, temperature and pressure information on each cell. It means that CEMA method is different from the computational singular perturbation (CSP) concept [57]. To further examine the nature of the flame, a local Damköhler number, Da, is shown in Fig. 16. Da is defined as:

$$\mathrm{Da} = \tau_f \times |\lambda_e| \tag{2}$$

where τ_f represents the integral time scale, which is calculated by $\tau_f = k/\varepsilon$. Distributions of T, Λ_e, and Da for double injections are shown in Fig. 16 with a long FID, i.e. (a) (b) and (c), and a short FID, i.e. (d) (e) and (f). The horizontal dashed line represents the position of flame lift-off length. It shows that two flame bases are located near the flame LOL. The transition for Λ_e at the position of flame LOL from a positive value to a negative value can also be observed in Fig. 16. For double injections, the flame LOL is reduced, and combustion of the second injection could extend to the upstream regions with higher scalar dissipation rates where high-temperature kernels couldn’t sustain for single injection [18]. It should be noted that CEM represents the reciprocal chemical time scale of a local mixture. The appearance of CEM implies that the corresponding mixture is explosive. In the upstream the flame surface regions, $Re(\lambda_e) > 0$, indicating that the mixture is explosive and autoignition is likely to occur without significant loss in heat and radicals. The previous results from the 1-D laminar simulations showed that a Da diffusive limit existed, below which, combustion of mixture was due to flame propagation without autoignition. Although the critical value of Da is changed with the fuel, it is in order of unity [44, 58, 59]. In the present work, for the cases with short

DT, for example with DT=0.5 ms, combustion of the first injection provides a high-temperature environment. Xu et al. [60] defined different zones in spray flames based on the eigenvalue distributions, namely the post-ignition zone with a negative value of λ_e, the premixed reaction fronts with $\lambda_e = 0$, the pre-ignition zone with a positive value of λ_e, and the chemically inactive zone with λ_e around zero. These zones can also be clearly seen in Fig. 16. Dark blue regions can be observed around the head of the second spray, indicating the already burnt region. At the regions upstream of the flame LOL, dark red regions are observed for the Λ_e contours, indicating a pre-ignition zone where the mixture is highly explosive. However, for the cases with short first injection durations, the increase in the dwell time leads to large differences in the distributions of Λ_e. As the injected fuel during the first injection is very less, the mixture ahead of the second spray at 0.6 ms ASSI becomes very lean. The temperature there is also very low (below 1000 K). The low temperature and lean mixture results in positive values of Λ_e. With the increase in DT, the mixture becomes much leaner and values of Λ_e at the regions ahead of the second spray decrease. Large Da in order of unity at the LOL is mainly distributed in the inner side of the spray, implying that the reaction and mixing process counterbalance each other. It indicates that the stabilization of the second injection is controlled by flame propagation. However, for a longer DT, more oxygen is entrained into the low-density regions after the combustion of the first injection. The influence of the combustion products from the first injection on the combustion of the second injection is reduced. No obvious flame front exists between the explosive and non-explosive mixture. As reported in the previous studies [58, 59], Da>1 indicates a dominant CEM state which is likely to induce actual autoignition. For the cases with long DTs, for example, DT=1.5 ms, Da at the location approaching the LOL is larger than unity, suggesting that the chemical reaction is much faster than the mixing. The chemical explosive process dominates the mixing, and thus, the mixture is autoigniting [61]. Similar phenomenon is also found in the lifted ethylene jet flame in highly-heated coflow using DNS [52, 56], where highly explosive mixtures are located near the injector. By increasing the interval between the two injections, the combustion of the first injection is more completed. Therefore, the main influence from the first injection is the temperature increase ahead of the second injection to promote the appearance of the explosive mixture, as shown in Figs. 16 (c) and (f), where high value of Da appears at the spray head of the second injection.

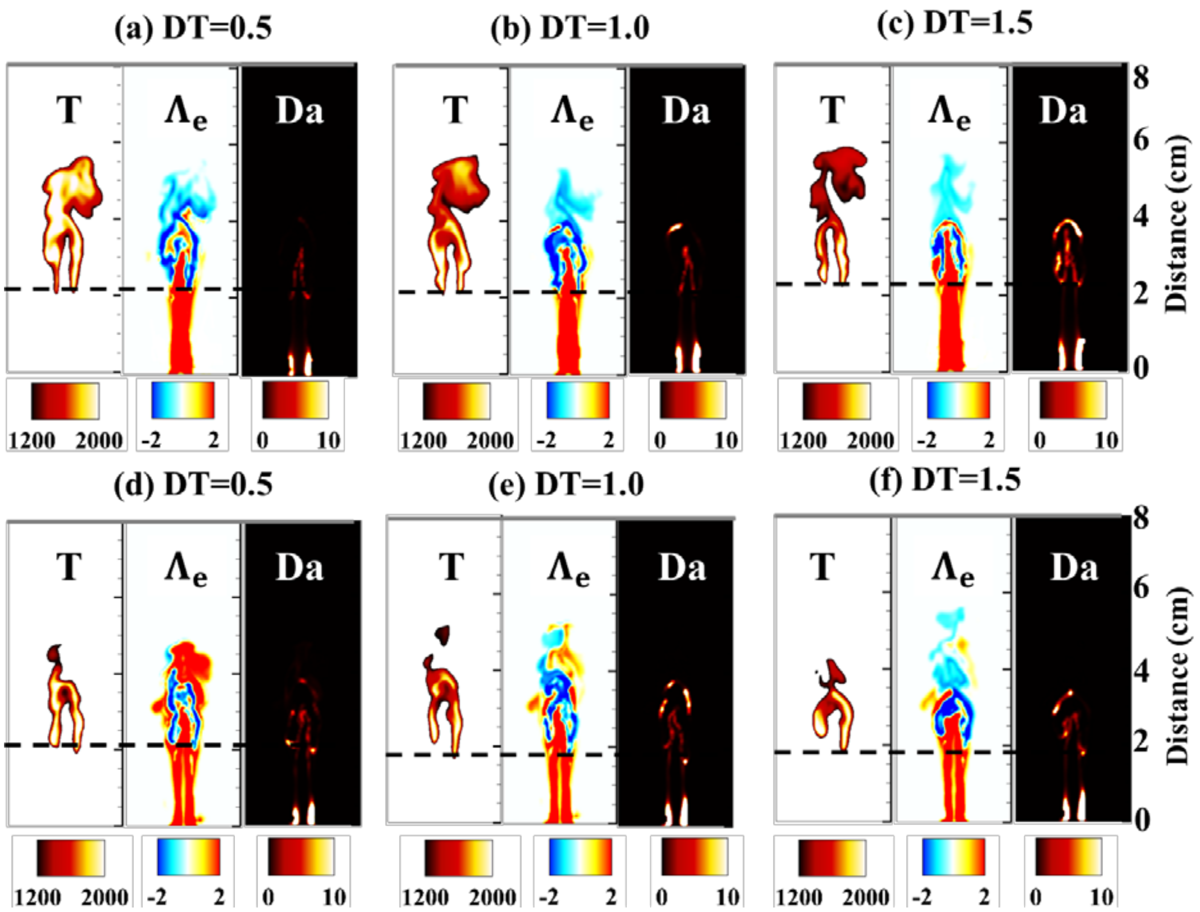

Fig. 16. Distributions of temperature (T), Λ_e and the Damköhler number (Da) at different dwell times. (a), (b) and (c): FID= 0.5 ms. (d), (e) and (f): FID= 0.3 ms. Λ_e is defined as $\Lambda_e = sign(Re(\lambda_e)) \times log_{10}(\max(1, Re(\lambda_e)))$, where 'sign' represents the sign function, and $Re(\lambda_e)$ is the real part of the largest non-zero eigenvalue. Time is at 0.6 ms ASSI. The horizontal dashed line represents the place of flame LOL.

4. Conclusions

In this work, combustion mechanisms of multiple injections are investigated using large eddy simulation (LES). A reduced mechanism including 54 species and 269 reactions for n-dodecane is used in this work. Good agreement between the predicted and measured data is observed in terms of the vapour penetration length. Moreover, the present models give reasonable prediction of species and density distributions compared with the experimental data. Analysis on the combustion process at different dwell times (DTs) and first injection durations show that the appearance of high-temperature kernels at long dwell time is delayed. This is because that the time for the second injection to come into contact with the combustion regions from the first injection is prolonged with a long DT. High-temperature reactions are initiated at fuel-rich regions for the first and second injections. Different ignition mechanisms are identified. Ignition of the first injection is controlled by autoignition, while the second injection is ignited by the first flame. Besides, the chemical explosive mode analysis (CEMA) method is used to interpret the stabilization mechanism. For the case with a short DT, the reaction and mixing balance occur simultaneously for the second injection, so the flame is stabilized because of flame propagation. For the case with a long DT, large values of Da are obtained, indicating that the chemical explosive mode dominates the mixing. The flame stabilization is controlled by autoignition. The interactions between the two reacting sprays are also discussed. The velocity of the second spray tip is obviously accelerated by the first reacting spray with a short DT. For the case with a long DT, fuel and intermediate species are almost consumed completely before the second tip catches up with the first one.

Acknowledgement

The work is supported by National Natural Science Foundation of China (Grant No. 91741119, 51606133, 91641203) and Marine Low-Speed Engine Project (Phase I). The work was carried out at National Supercomputer Center in Tianjin, and the calculations were performed on TianHe-1 (A).

We declare that we have no conflict of interest.

References

[1] R.D. Reitz, Directions in internal combustion engine research, Combust. Flame 160 (2013) 1-8.

[2] A.K. Agarwal, A.P. Singh, R.K. Maurya, Evolution, challenges and path forward for low temperature combustion engines, Prog. Energy Combust. Sci. 61 (2017) 1-56.

[3] M. Yao, Z. Zheng, H. Liu, Progress and recent trends in homogeneous charge compression ignition (HCCI) engines, Prog. Energy Combust. Sci. 35 (2009) 398-437.

[4] M.P.B. Musculus, P.C. Miles, L.M. Pickett, Conceptual models for partially premixed low-temperature diesel combustion, Prog. Energy Combust. Sci. 39 (2013) 246-283.

[5] A. Wehrfritz, O. Kaario, V. Vuorinen, B. Somers, Large Eddy Simulation of n-dodecane spray flames using Flamelet Generated Manifolds, Combust. Flame 167 (2016) 113-131.

[6] A. Jain, A.P. Singh, A.K. Agarwal, Effect of split fuel injection and EGR on NOx and PM emission reduction in a low temperature combustion (LTC) mode diesel engine, Energy 122 (2017) 249-264.

[7] K. Han, B. Jang, G. Lakew, K.Y. Huh, Combustion Simulation of a Diesel Engine with Split Injections by Lagrangian Conditional Moment Closure Model, Combust. Sci. Technol. 190 (2018) 1-19.
[8] A.A. Moiz, K.D. Cung, S.-Y. Lee, Simultaneous Schlieren–PLIF Studies for Ignition and Soot Luminosity Visualization With Close-Coupled High-Pressure Double Injections of n-Dodecane, Journal of Energy Resources Technology 139 (2017) 012207-012207-012212.
[9] Z. Zheng, L. Yue, H. Liu, Y. Zhu, X. Zhong, M. Yao, Effect of two-stage injection on combustion and emissions under high EGR rate on a diesel engine by fueling blends of diesel/gasoline, diesel/n-butanol, diesel/gasoline/n-butanol and pure diesel, Energy Convers. Manage. 90 (2015) 1-11.
[10] X.-R. Li, W. Yang, L.-M. Zhao, F.-S. Liu, The influence of pilot-main injection matching on DI diesel engine combustion using an endoscopic visualization system, Fuel 188 (2017) 575-585.
[11] S. Skeen, J. Manin, L.M. Pickett, Visualization of Ignition Processes in High-Pressure Sprays with Multiple Injections of n-Dodecane, SAE Int. J. Engines 8 (2015) 696-715.
[12] M. Bolla, M.A. Chishty, E.R. Hawkes, S. Kook, Modeling combustion under engine combustion network Spray A conditions with multiple injections using the transported probability density function method, Int. J. Engine Res. 18 (2017) 6-14.
[13] M.R. Herfatmanesh, P. Lu, M.A. Attar, H. Zhao, Experimental investigation into the effects of two-stage injection on fuel injection quantity, combustion and emissions in a high-speed optical common rail diesel engine, Fuel 109 (2013) 137-147.
[14] K. Cung, A. Moiz, J. Johnson, S.-Y. Lee, C.-B. Kweon, A. Montanaro, Spray–combustion interaction mechanism of multiple-injection under diesel engine conditions, Proc. Combust. Inst. 35 (2015) 3061-3068.
[15] A.A. Moiz, K.D. Cung, S.-Y. Lee, Ignition, lift-off, and soot formation studies in n-dodecane split injection spray-flames, Int. J. Engine Res. 18 (2017) 1077-1087.
[16] A.A. Moiz, M.M. Ameen, S.-Y. Lee, S. Som, Study of soot production for double injections of n-dodecane in CI engine-like conditions, Combust. Flame 173 (2016) 123-131.
[17] C. Hasse, N. Peters, A two mixture fraction flamelet model applied to split injections in a DI Diesel engine, Proc. Combust. Inst. 30 (2005) 2755-2762.
[18] C. Felsch, M. Gauding, C. Hasse, S. Vogel, N. Peters, An extended flamelet model for multiple injections in DI Diesel engines, Proc. Combust. Inst. 32 (2009) 2775-2783.
[19] J. Lim, S. Lee, K. Min, Combustion Modeling of Split Injection in HSDI Diesel Engines, Combust. Sci. Technol. 183 (2010) 180-201.
[20] C.K. Blomberg, L. Zeugin, S.S. Pandurangi, M. Bolla, K. Boulouchos, Y.M. Wright, Modeling Split Injections of ECN “Spray A” Using a Conditional Moment Closure Combustion Model with RANS and LES, SAE Int. J. Engines 9 (2016) 2107-2119.
[21] L.M. Pickett, Engine Combustion Network <http://www.sandia.gov/ecn/>. (2012).
[22] A.A. Amsden, KIVA3V: a block-structured KIVA program for engines with vertical or canted valves, Los Alamos, (1997).
[23] B. van Leer, Towards the ultimate conservative difference scheme. II. Monotonicity and conservation combined in a second-order scheme, Journal of Computational Physics 14 (1974) 361-370.
[24] L. Zhou, K.H. Luo, W. Qin, M. Jia, S.J. Shuai, Large eddy simulation of spray and combustion characteristics with realistic chemistry and high-order numerical scheme under diesel engine-like conditions, Energy Convers. Manage. 93 (2015) 377-387.
[25] K. Sone, S. Menon, Effect of Subgrid Modeling on the In-Cylinder Unsteady Mixing Process in a Direct Injection Engine, J. Eng. Gas Turbines Power 125 (2003) 435-443.
[26] N. Patel, S. Menon, Simulation of spray–turbulence–flame interactions in a lean direct injection combustor, Combust. Flame 153 (2008) 228-257.
[27] B.A. Sen, S. Menon, Turbulent premixed flame modeling using artificial neural networks based chemical kinetics, Proc. Combust. Inst. 32 (2009) 1605-1611.
[28] H. El-Asrag, S. Menon, Large eddy simulation of soot formation in a turbulent non-premixed jet flame, Combust. Flame 156 (2009) 385-395.
[29] H. Wei, W. Zhao, L. Zhou, C. Chen, G. Shu, Large eddy simulation of the low temperature ignition and combustion processes on spray flame with the linear eddy model, Combust. Theory Modell. 22 (2018) 237-263.
[30] L. Zhou, W. Zhao, H. Wei, Large Eddy Simulation on the Flame Structure for Split Injections of n-dodecane at Different Temperatures and Densities, Combust. Sci. Technol. 190 (2018) 2224-2244.
[31] T. Yao, Y. Pei, B.-J. Zhong, S. Som, T. Lu, K.H. Luo, A compact skeletal mechanism for n-dodecane with optimized semi-global low-temperature chemistry for diesel engine simulations, Fuel 191 (2017) 339-349.
[32] S.F. Fernandez, C. Paul, A. Sircar, A. Imren, D.C. Haworth, S. Roy, M.F. Modest, Soot and spectral radiation modeling for high-pressure turbulent spray flames, Combust. Flame 190 (2018) 402-415.
[33] M. Bolla, M.A. Chishty, E.R. Hawkes, Q.N. Chan, S. Kook, Influence of turbulent fluctuations on radiation heat transfer, NO and soot formation under ECN Spray A conditions, Proc. Combust. Inst. 36 (2017) 3551-3558.
[34] M.A. Chishty, M. Bolla, E.R. Hawkes, Y. Pei, S. Kook, Soot formation modelling for n-dodecane sprays using the transported PDF model, Combust. Flame 192 (2018) 101-119.
[35] M.A. Patterson, R.D. Reitz, Modeling the Effects of Fuel Spray Characteristics on Diesel Engine Combustion and

Emission, SAE International, 1998.

[36] P.J. O'Rourke, Collective Drop Effects on Vaporizing Liquid Sprays, Engineering, (1981).

[37] L. Zhou, M. Xie, M. Jia, Q. Zhou, C. Xu. Influences of subgrid turbulent kinetic energy and turbulent dispersion on the characteristics of fuel spray. In: editor^editors. SAE Technical Papers. 2011: SAE International. p.

[38] N. Bharadwaj, C.J. Rutland, S. Chang, Large eddy simulation modelling of spray-induced turbulence effects, Int. J. Engine Res. 10 (2009) 97-119.

[39] H. Wei, W. Zhao, L. Zhou, G. Shu, Numerical investigation of diesel spray flame structures under diesel engine-relevant conditions using large eddy simulation, Combust. Sci. Technol. 190 (2018) 909-932.

[40] C. Bekdemir, L.M.T. Somers, L.P.H. de Goey, J. Tillou, C. Angelberger, Predicting diesel combustion characteristics with Large-Eddy Simulations including tabulated chemical kinetics, Proc. Combust. Inst. 34 (2013) 3067-3074.

[41] S.A. Skeen, J. Manin, L.M. Pickett, Simultaneous formaldehyde PLIF and high-speed schlieren imaging for ignition visualization in high-pressure spray flames, Proc. Combust. Inst. 35 (2015) 3167-3174.

[42] G. Borghesi, E. Mastorakos, R.S. Cant, Complex chemistry DNS of n-heptane spray autoignition at high pressure and intermediate temperature conditions, Combust. Flame 160 (2013) 1254-1275.

[43] A. Irannejad, A. Banaeizadeh, F. Jaberi, Large eddy simulation of turbulent spray combustion, Combust. Flame 162 (2015) 431-450.

[44] M.B. Luong, G.H. Yu, S.H. Chung, C.S. Yoo, Ignition of a lean PRF/air mixture under RCCI/SCCI conditions: Chemical aspects, Proc. Combust. Inst. 36 (2017) 3587-3596.

[45]
J.M. Desantes, J. Arregle, J.J. Lopez, A. Garcia. A comprehensive study of diesel combustion and emissions with post-injection. In: editor^editors. SAE Technical Papers. 2007 World Congress, April 16, 2007 - April 19, 2007; 2007; Detroit, MI, United states: SAE International. p.

[46] L. Ma, D. Roekaerts, Structure of spray in hot-diluted coflow flames under different coflow conditions: A numerical study, Combust. Flame 172 (2016) 20-37.

[47] L. Ma, D. Roekaerts, Numerical study of the multi-flame structure in spray combustion, Proc. Combust. Inst. 36 (2017) 2603-2613.

[48] J.M. Desantes, J.V. Pastor, J.M. García-Oliver, F.J. Briceño, An experimental analysis on the evolution of the transient tip penetration in reacting Diesel sprays, Combust. Flame 161 (2014) 2137-2150.

[49] CHEMKIN-PRO 15131, Reaction Design: San Diego, (2013).

[50] J.M. Desantes, J.M. García-Oliver, A. García, T. Xuan, Optical study on characteristics of non-reacting and reacting diesel spray with different strategies of split injection, Int. J. Engine Res. 0 (2018) 1468087418773012.

[51] A. Hadadpour, M. Jangi, X.S. Bai, The Effect of Splitting Timing on Mixing in a Jet with Double Injections, Flow Turbulence and Combustion, doi:https://doi.org/10.1007/s10494-018-9904-8(2018).

[52] Z. Luo, C.S. Yoo, E.S. Richardson, J.H. Chen, C.K. Law, T. Lu, Chemical explosive mode analysis for a turbulent lifted ethylene jet flame in highly-heated coflow, Combust. Flame 159 (2012) 265-274.

[53] R. Shan, C.S. Yoo, J.H. Chen, T. Lu, Computational diagnostics for n-heptane flames with chemical explosive mode analysis, Combust. Flame 159 (2012) 3119-3127.

[54] Y. Minamoto, H. Kolla, R.W. Grout, A. Gruber, J.H. Chen, Effect of fuel composition and differential diffusion on flame stabilization in reacting syngas jets in turbulent cross-flow, Combust. Flame 162 (2015) 3569-3579.

[55] Z. Lu, H. Zhou, S. Li, Z. Ren, T. Lu, C.K. Law, Analysis of operator splitting errors for near-limit flame simulations, Journal of Computational Physics 335 (2017) 578-591.

[56] C.S. Yoo, E.S. Richardson, R. Sankaran, J.H. Chen, A DNS study on the stabilization mechanism of a turbulent lifted ethylene jet flame in highly-heated coflow, Proc. Combust. Inst. 33 (2011) 1619-1627.

[57] C. Xu, J.-W. Park, C.S. Yoo, J.H. Chen, T. Lu, Identification of premixed flame propagation modes using chemical explosive mode analysis, Proc. Combust. Inst. 37 (2019) 2407-2415.

[58] M.B. Luong, T. Lu, S.H. Chung, C.S. Yoo, Direct numerical simulations of the ignition of a lean biodiesel/air mixture with temperature and composition inhomogeneities at high pressure and intermediate temperature, Combust. Flame 161 (2014) 2878-2889.

[59] M.B. Luong, G.H. Yu, T. Lu, S.H. Chung, C.S. Yoo, Direct numerical simulations of ignition of a lean n-heptane/air mixture with temperature and composition inhomogeneities relevant to HCCI and SCCI combustion, Combust. Flame 162 (2015) 4566-4585.

[60] C. Xu, M.M. Ameen, S. Som, J.H. Chen, Z. Ren, T. Lu, Dynamic adaptive combustion modeling of spray flames based on chemical explosive mode analysis, Combust. Flame 195 (2018) 30-39.

[61] C.S. Yoo, T. Lu, J.H. Chen, C.K. Law, Direct numerical simulations of ignition of a lean n-heptane/air mixture with temperature inhomogeneities at constant volume: Parametric study, Combust. Flame 158 (2011) 1727-1741.